



A binuclear Co-based metal–organic framework towards efficient oxygen evolution reaction†

 Ning Liu, QiaoQiao Zhang and Jingqi Guan *

 Cite this: *Chem. Commun.*, 2021, 57, 5016

 Received 19th March 2021,
Accepted 14th April 2021

DOI: 10.1039/d1cc01492g

rsc.li/chemcomm

The search for low-cost and high-performance electrocatalysts for oxygen evolution reaction (OER) has aroused enormous research interest in the last few years. Reported herein is the topotactic construction of a binuclear Co-based metal–organic framework (Co₂-tzpa) using a solvothermal reaction. Prominently, as a porous catalyst, Co₂-tzpa holds its activity for at least 25 hours and exhibits low OER overpotentials of 336 and 396 mV to achieve the current density of 10 mA cm⁻² in 1 M KOH and 0.1 M KOH, respectively. The excellent OER performance should be attributed to each cobalt site coordinated with two tetrazolate N atoms.

The oxygen evolution reaction (OER) is the core of many renewable energy technologies (*e.g.* electrolysis of water, electrocatalytic CO₂ reduction, rechargeable fuel cells and metal–air batteries), by which electrical energy can be converted into chemical energy in fuels and chemicals.^{1,2} However, the slow dynamics of the OER hinders significantly the commercial applications of these technologies.³ Fabricating high-performance and robust electrocatalysts in the light of rational design fundamentals is the key to improve energy utilization.^{4–6} Metal–organic framework (MOF) materials with a high surface area, isolated active sites, and structural tailorability that provide a large number of active sites are regarded as promising candidates for various energy conversion and storage systems.^{7–10} However, most MOFs exhibit poor electrical conductivity and electrochemical activity (especially inferior OER activity), which make them restricted in electrochemical water splitting.¹¹

There are some strategies to improve the electrocatalytic activity of MOFs, such as dual-site mechanism,^{12,13} surface hydroxylation,¹⁴ defects,¹⁵ and lattice contraction.¹⁶ Nevertheless, the intrinsic activity of MOFs should be related to the kind of metal site and their electronic structure. Up to now, Co-based,^{17,18} Ni-based,^{19–22} Cu-based,²³ Zn-based,²⁴ Pb-based,²⁵

and bimetallic MOFs^{13,26,27} have been reported to be active for OER. Thereinto, Co-based MOFs have gained considerable research interest due to their high activity and structural stability.²⁸ The electronic structure of Co sites is primarily influenced by the topological structure of MOFs and their coordination environment.²⁹ Different nuclear Co-based MOFs have been synthesized for OER, such as mononuclear,³⁰ binuclear,³¹ trinuclear,³² tetranuclear,³³ and hexanuclear.³⁴ Compared with mononuclear MOFs, multinuclear MOFs possess multiple active sites, which can synergistically catalyze the OER to lower the reaction barrier. Compared to N-containing Co-based MOFs, Co-based MOFs fabricated with N-free ligands usually show worse OER activity. For example, Oña-Burgos *et al.* reported a N-free Co₂-MOF, which showed a high OER overpotential of 626 mV in 0.1 M sodium phosphate buffer solution.³¹ To regulate the electronic configuration of Co sites and enhance the electrocatalytic activity, N-containing ligands were frequently used for fabricating MOFs. For instance, a N-ligand containing [Co₂(μ-OH)₂(bbta)] exhibited an overpotential of 292 mV for OER in alkaline media.¹⁴

Although more than 88 000 kinds of MOFs have been successfully fabricated and used in various fields, a very limited number of Co-based MOFs are directly used as active OER electrocatalysts.³⁵ Compared with other Co-based catalysts, Co-based MOFs have some advantages for OER, such as regular and adjustable active sites, porous structure, *etc.* Herein, we report a binuclear Co-based MOF with each Co atom coordinated with two tetrazolate N atoms, which can efficiently catalyze OER in alkaline media. We expect this work may be conducive to fabricating more MOFs for OER.

The binuclear Co-based MOF (Co₂-tzpa) can be synthesized by reacting Co²⁺ ions with 5-(4-(tetrazol-5-yl)phenyl)isophthalic acid (H₃tzpa) under solvothermal conditions as described in Fig. 1a.³⁶ XRD patterns show that all the characteristic peaks of the as-prepared sample can be well matched with the simulated ones (Fig. 1b), indicating that the binuclear Co-MOF (Co₂-tzpa) was successfully synthesized. The cobalt ions are coordinated with two tetrazolate N atoms. Moreover, the Co^{1#} center is

Institute of Physical Chemistry, College of Chemistry, Jilin University, Changchun 130021, P. R. China. E-mail: guanjq@jlu.edu.cn

† Electronic supplementary information (ESI) available. See DOI: 10.1039/d1cc01492g

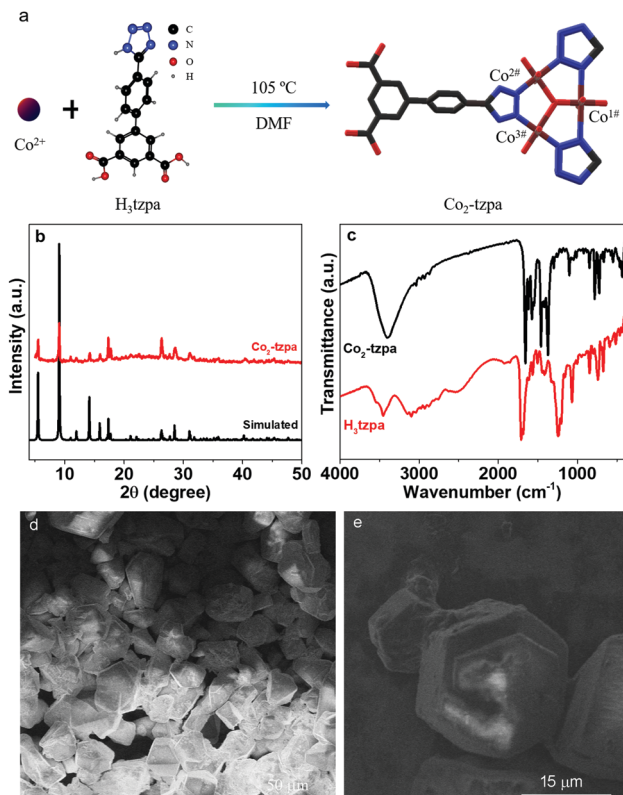


Fig. 1 (a) Synthetic procedure of $\text{Co}_2\text{-tzpa}$. (b) XRD patterns of experimental and simulated $\text{Co}_2\text{-tzpa}$. (c) FT-IR spectra of H_3tzpa and $\text{Co}_2\text{-tzpa}$. (d and e) SEM images of $\text{Co}_2\text{-tzpa}$ with different amplifications.

encircled by additional three COO^- and one HO^- , while both $\text{Co}^{2\#}$ and $\text{Co}^{3\#}$ are anchored by additional two HO^- and two H_2O molecules located at the two axial apexes of an octahedron. The successful fabrication of Co-MOF can be further verified by the FT-IR spectra. As depicted in Fig. 1c, the main peaks at 669, 736, 844, 1063, 1238, and 1711 cm^{-1} ascribed to the H_3tzpa parent disappear, and new peaks at 720, 782, 849, 1097, 1373, 1458, and 1655 cm^{-1} appear for the $\text{Co}_2\text{-tzpa}$, suggesting that the cobalt ions are coordinated with the H_3tzpa , which influence the vibrations of the C-C, C-N, and C-O bonds. The morphology of $\text{Co}_2\text{-tzpa}$ was examined by SEM. As shown in Fig. 1d and e, typical block structures with a length of 10–40 μm and thickness of $\sim 6 \mu\text{m}$ can be observed. The BET surface area of $\text{Co}_2\text{-tzpa}$ is approximately $228.7 \text{ m}^2 \text{ g}^{-1}$ and the pore diameter is about 3.8 nm (Fig. S1, ESI †). The porous structure of $\text{Co}_2\text{-tzpa}$ can be further verified using the TEM image (Fig. S2, ESI †).

The chemical compositions and valence state of cobalt were analyzed by XPS. As demonstrated in Fig. 2, the survey spectrum manifests the presence of C, N, O, and Co elements in $\text{Co}_2\text{-tzpa}$. The high-resolution C 1s spectrum can be deconvoluted to two peaks centered at *ca.* 284.6 and 285.5 eV (Fig. 2b), ascribed to the C-C and C-N bonds, respectively.³⁷ The N 1s XPS spectrum can be deconvoluted to three peaks at 400.8, 400.3, and 399.6 eV (Fig. 2c), corresponding to Co-N, N=N and C-N coordination, respectively.^{38,39} In the Co 2p spectrum, the peak positions of Co $2p_{3/2}$ and Co $2p_{1/2}$ are centered at 781.0

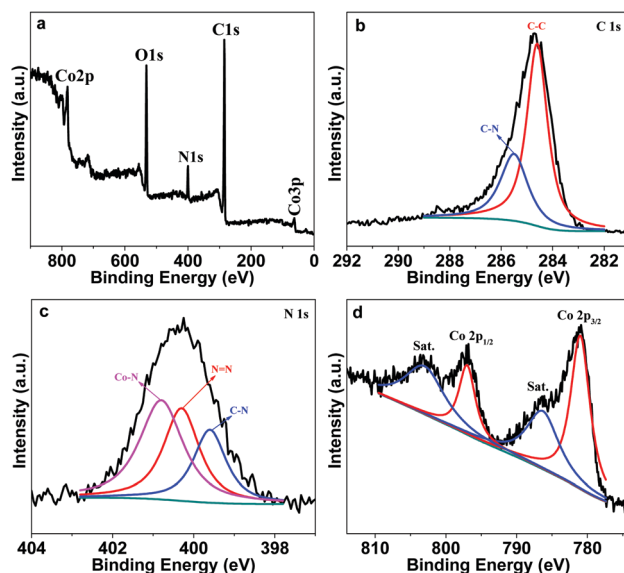


Fig. 2 (a) XPS survey spectrum. (b–d) High resolution XPS spectra for (b) C 1s, (c) N 1s, and (d) Co 2p regions of $\text{Co}_2\text{-tzpa}$.

and 797.0 eV, respectively, along with two satellite peaks centered at 786.5 and 803.2 eV (Fig. 2d), indicating that the cobalt ions in the sample have charge of plus two.

The OER performance was first evaluated in 1 M KOH. For comparison, nano Co_3O_4 with an average particle size of $\sim 5 \text{ nm}$ was synthesized using a hydrothermal method.⁴⁰ As shown in Fig. 3a, the nano Co_3O_4 shows a relatively poor OER performance with an overpotential (η_{10}) of 388 mV at the current density of 10 mA cm^{-2} . In stark contrast, $\text{Co}_2\text{-tzpa}$ is markedly active for the OER with a low overpotential of 336 mV, and additional positive potential leads to the rapid increase of the anodic current, which can be compared with commercial

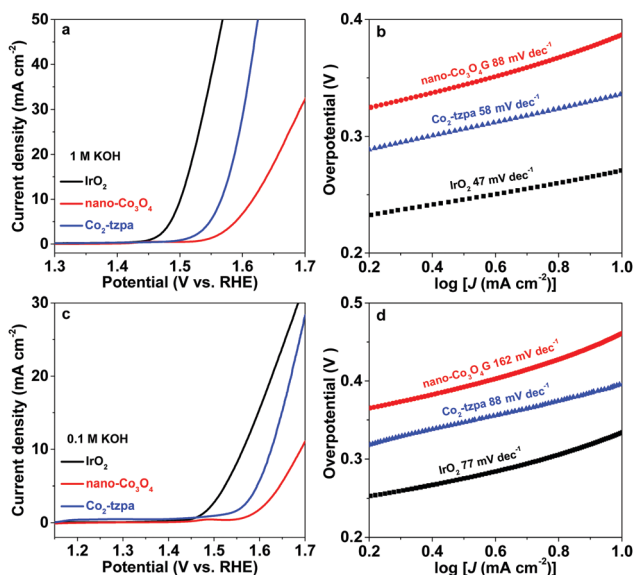


Fig. 3 (a) OER polarization curves and (b) Tafel plots in 1 M KOH. (c) OER polarization curves and (d) Tafel plots in 0.1 M KOH.

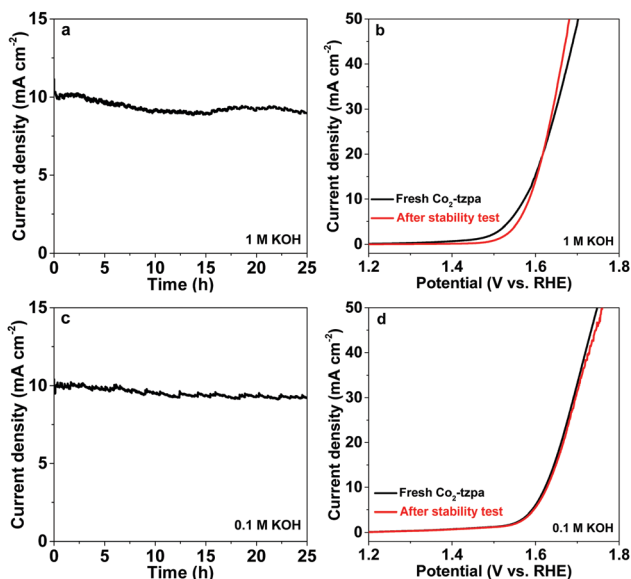


Fig. 4 (a) Chronoamperometric measurement in 1 M KOH. (b) OER polarization curves without iR-compensation. (c) Chronoamperometric measurement in 0.1 M KOH. (d) OER polarization curves.

IrO₂ catalysts. In addition, the OER activity of Co₂-tzpa can be compared to that of most MOF-based catalysts in alkaline media (Table S1, ESI[†]). The Tafel slopes are *ca.* 47, 88, and 58 mV dec⁻¹ for IrO₂, Co₃O₄, and Co₂-tzpa, respectively (Fig. 3b). The Tafel slope for Co₂-tzpa reveals the OER rate-limiting step following the first electron transfer.⁴¹

The OER performance of Co₂-tzpa was further evaluated in 0.1 M KOH. As displayed in Fig. 3c, Co₂-tzpa needs an η_{10} of 396 mV, much smaller than nano Co₃O₄ (461 mV) and slightly higher than commercial IrO₂ (334 mV). The Tafel slopes are 77, 162, and 88 mV dec⁻¹ for IrO₂, Co₃O₄, and Co₂-tzpa, respectively (Fig. 3d).

The electrochemical surface area can be used to reflect the surface roughness of the electrocatalysts, which can be measured by the capacitance of the double layer.^{42,43} As exhibited in Fig. S3 and S4 (ESI[†]), the electrochemical surface area of Co₂-tzpa is 811 cm², which is far larger than that of nano-Co₃O₄ (only 24 cm²), indicating that more active sites are generated on the former. Moreover, we performed electrochemical impedance spectroscopy (EIS) to estimate charge transfer resistance (R_{ct}). As revealed in Fig. S5–S8 (ESI[†]), Co₂-tzpa shows a smaller R_{ct} than Co₃O₄, implying favorable OER kinetics. The OER energy barrier (ΔG) on Co₂-tzpa can be derived from the following eqn (1)–(4),

$$i = i_0 \times e^{\frac{(1-\alpha)F(E-E_0)}{RT}} \quad (1)$$

$$k = Ae^{\frac{-\Delta G}{RT}} \quad (2)$$

$$\Delta G = (1 - \alpha)nFE_0 - (1 - \alpha)nFE \quad (3)$$

$$\alpha = \frac{1}{1 + \frac{-a_1}{a_2}} \quad (4)$$

where T is the experimental temperature, R is gas constant (8.314 J mol⁻¹ k⁻¹), n is the electron transfer number ($n = 4$), F is Faraday constant (96 485 C mol⁻¹), J_0 is the exchange current density, a is the Tafel slope, and α is obtained from the Tafel slopes. When the imposed potential E_0 is 0 V, ΔG is estimated to be *ca.* 347 kJ mol⁻¹.

The durability of Co₂-tzpa was assessed by supporting it on a graphite plate in 1 M KOH and 0.1 M KOH solutions. As shown in Fig. 4, after a long period of operation (25 h), it was observed that the current density only exhibits slight degradation in the two kinds of electrolytes, which could be due to the obstacle of the reaction by oxygen bubbles that remained on Co₂-tzpa. The OER polarization curves show a negligible difference compared with the initial ones, further suggesting the outstanding durability of Co₂-tzpa under alkaline OER conditions. The faradaic efficiency is measured to be >98%, demonstrating the high-efficiency OER performance of Co₂-tzpa (Fig. S9, ESI[†]). The high OER activity of Co₂-tzpa can be attributed to the cobalt ions coordinated with two nitrogen atoms, which was theoretically predicted to be more active for OER than Co₃O₄ and CoOOH in our previous work.³⁸ The O* intermediate is more stable on the Co-N₂ site than on Co₃O₄ and CoOOH, leading to a lower energy barrier on the former.^{38,44} The high stability of Co₂-tzpa can be ascribed to the cobalt ions immobilized by the metal-organic framework. XPS measurements reveal that the Co was completely oxidized from initial +2 to +3 during the durability tests (Fig. S10, ESI[†]), indicating that Co³⁺ is a key intermediate for OER.

In conclusion, a binuclear Co₂-tzpa catalyst was successfully synthesized using a solvothermal method, where each cobalt ion is coordinated with two tetrazolate N atoms. The Co₂-tzpa shows high activity and durability for OER in alkaline aqueous solutions. In 1 M KOH and 0.1 M KOH, the Co₂-tzpa needs overpotentials of 336 and 396 mV to achieve the current density of 10 mA cm⁻², respectively. The enhanced OER activity of Co₂-tzpa can be attributed to the nitrogen-coordination effect, while the metal-organic framework favors the improvement of its catalytic stability.

This work was supported by the National Natural Science Foundation of China (22075099), Natural Science Foundation of Jilin Province (20180101291JC).

Conflicts of interest

There are no conflicts to declare.

Notes and references

- H. Xu, D. Cheng, D. Cao and X. C. Zeng, *Nat. Catal.*, 2018, **1**, 339–348.
- H. Chen, X. Liang, Y. Liu, X. Ai, T. Asefa and X. Zou, *Adv. Mater.*, 2020, **32**, 2002435.
- Q. Zhang and J. Guan, *Adv. Funct. Mater.*, 2020, **30**, 2000768.
- S. Li, J. Sun and J. Guan, *Chin. J. Catal.*, 2021, **42**, 511–556.

- 5 L. Wang, Z. Li, K. Wang, Q. Dai, C. Lei, B. Yang, Q. Zhang, L. Lei, M. K. H. Leung and Y. Hou, *Nano Energy*, 2020, **74**, 104850.
- 6 C. Lei, S. Lyu, J. Si, B. Yang, Z. Li, L. Lei, Z. Wen, G. Wu and Y. Hou, *ChemCatChem*, 2019, **11**, 5855–5874.
- 7 A. Dhakshinamoorthy, A. M. Asiri and H. Garcia, *Angew. Chem., Int. Ed.*, 2016, **55**, 5414–5445.
- 8 J.-Y. Xue, C. Li, F.-L. Li, H.-W. Gu, P. Braunstein and J.-P. Lang, *Nanoscale*, 2020, **12**, 4816–4825.
- 9 B. Zhu, Z. Liang, D. Xia and R. Zou, *Energy Storage Mater.*, 2019, **23**, 757–771.
- 10 K. Zhao, W. Zhu, S. Liu, X. Wei, G. Ye, Y. Su and Z. He, *Nanoscale Adv.*, 2020, **2**, 536–562.
- 11 J. Song, C. Wei, Z.-F. Huang, C. Liu, L. Zeng, X. Wang and Z. J. Xu, *Chem. Soc. Rev.*, 2020, **49**, 2196–2214.
- 12 J.-Q. Shen, P.-Q. Liao, D.-D. Zhou, C.-T. He, J.-X. Wu, W.-X. Zhang, J.-P. Zhang and X.-M. Chen, *J. Am. Chem. Soc.*, 2017, **139**, 1778–1781.
- 13 X.-L. Wang, L.-Z. Dong, M. Qiao, Y.-J. Tang, J. Liu, Y. Li, S.-L. Li, J.-X. Su and Y.-Q. Lan, *Angew. Chem., Int. Ed.*, 2018, **57**, 9660–9664.
- 14 X.-F. Lu, P.-Q. Liao, J.-W. Wang, J. X. Wu, X.-W. Chen and C.-T. He, *J.-P. Zhang, G.-R. Li and X.-M. Chen, J. Am. Chem. Soc.*, 2016, **138**, 8336–8339.
- 15 Z. Xue, K. Liu, Q. Liu, Y. Li, M. Li, C.-Y. Su, N. Ogiwara, H. Kobayashi, H. Kitagawa, M. Liu and G. Li, *Nat. Commun.*, 2019, **10**, 5048.
- 16 W. Cheng, X. Zhao, H. Su, F. Tang, W. Che, H. Zhang and Q. Liu, *Nat. Energy*, 2019, **4**, 115–122.
- 17 R. K. Tripathy, A. K. Samantara and J. N. Behera, *Dalton Trans.*, 2019, **48**, 10557–10564.
- 18 J. Jiang, L. Huang, X. Liu and L. Ai, *ACS Appl. Mater. Interfaces*, 2017, **9**, 7193–7201.
- 19 X. Wang, B. Li, Y.-P. Wu, A. Tsamis, H.-G. Yu, S. Liu, J. Zhao, Y.-S. Li and D.-S. Li, *Inorg. Chem.*, 2020, **59**, 4764–4771.
- 20 P. He, Y. Xie, Y. Dou, J. Zhou, A. Zhou, X. Wei and J.-R. Li, *ACS Appl. Mater. Interfaces*, 2019, **11**, 41595–41601.
- 21 F. Cheng, Z. Li, L. Wang, B. Yang, J. Lu, L. Lei, T. Ma and Y. Hou, *Mater. Horiz.*, 2021, **8**, 556–564.
- 22 F. Cheng, L. Wang, H. Wang, C. Lei, B. Yang, Z. Li, Q. Zhang, L. Lei, S. Wang and Y. Hou, *Nano Energy*, 2020, **71**, 104621.
- 23 J. Rong, F. Qiu, T. Zhang, Y. Fang, J. Xu and Y. Zhu, *Electrochim. Acta*, 2019, **313**, 179–188.
- 24 W. Pang, B. Shao, X.-Q. Tan, C. Tang, Z. Zhang and J. Huang, *Nanoscale*, 2020, **12**, 3623–3629.
- 25 F. Dai, W. Fan, J. Bi, P. Jiang, D. Liu, X. Zhang, H. Lin, C. Gong, R. Wang, L. Zhang and D. Sun, *Dalton Trans.*, 2016, **45**, 61–65.
- 26 M. Gu, S.-C. Wang, C. Chen, D. Xiong and F.-Y. Yi, *Inorg. Chem.*, 2020, **59**, 6078–6086.
- 27 W.-C. Hu, Y. Shi, Y. Zhou, C. Wang, M. R. Younis, J. Pang, C. Wang and X.-H. Xia, *J. Mater. Chem. A*, 2019, **7**, 10601–10609.
- 28 Q. Shi, S. Fu, C. Zhu, J. Song, D. Du and Y. Lin, *Mater. Horiz.*, 2019, **6**, 684–702.
- 29 E. A. Dolgoplova, A. J. Brandt, O. A. Ejegbavwo, A. S. Duke, T. D. Maddumapatabandi, R. P. Galhenage, B. W. Larson, O. G. Reid, S. C. Ammal, A. Heyden, M. Chandrasekhar, V. Stavila, D. A. Chen and N. B. Shustova, *J. Am. Chem. Soc.*, 2017, **139**, 5201–5209.
- 30 L. Yaqoob, T. Noor, N. Iqbal, H. Nasir, M. Sohail, N. Zaman and M. Usman, *Renewable Energy*, 2020, **156**, 1040–1054.
- 31 S. Gutierrez-Tarrino, J. Luis Olloqui-Sariego, J. Jose Calvente, M. Palomino, G. Minguez Espallargas, J. L. Jorda, F. Rey and P. Ona-Burgos, *ACS Appl. Mater. Interfaces*, 2019, **11**, 46658–46665.
- 32 M. Zhang, B.-H. Zheng, J. Xu, N. Pan, J. Yu, M. Chen and H. Cao, *Chem. Commun.*, 2018, **54**, 13579–13582.
- 33 X. Song, C. Peng and H. Fei, *ACS Appl. Energy Mater.*, 2018, **1**, 2446–2451.
- 34 J.-W. Tian, Y.-P. Wu, Y.-S. Li, J.-H. Wei, J.-W. Yi, S. Li, J. Zhao and D.-S. Li, *Inorg. Chem.*, 2019, **58**, 5837–5843.
- 35 D. Zhu, M. Qiao, J. Liu, T. Tao and C. Guo, *J. Mater. Chem. A*, 2020, **8**, 8143–8170.
- 36 H.-H. Wang, L. Hou, Y.-Z. Li, C.-Y. Jiang, Y.-Y. Wang and Z. Zhu, *ACS Appl. Mater. Interfaces*, 2017, **9**, 17969–17976.
- 37 Q. Zhang, Z. Duan, Y. Wang, L. Li, B. Nan and J. Guan, *J. Mater. Chem. A*, 2020, **8**, 19665–19673.
- 38 Q. Zhang, Z. Duan, M. Li and J. Guan, *Chem. Commun.*, 2019, **56**, 794–797.
- 39 W. Luo, W. Li, J. Tan, J. Liu, B. Tan, X. Zuo, Z. Wang and X. Zhang, *J. Mol. Liq.*, 2020, **314**, 113630.
- 40 Y. Dong, K. He, L. Yin and A. Zhang, *Nanotechnology*, 2007, **18**, 435602.
- 41 M. S. Burke, M. G. Kast, L. Trotochaud, A. M. Smith and S. W. Boettcher, *J. Am. Chem. Soc.*, 2015, **137**, 3638–3648.
- 42 C. C. McCrory, S. Jung, J. C. Peters and T. F. J. J. O. T. A. C. S. Jaramillo, *J. Am. Chem. Soc.*, 2015, **137**, 3638–3648.
- 43 H. Fei, J. Dong, M. J. Arellano-Jiménez, G. Ye, N. Dong Kim, E. L. G. Samuel, Z. Peng, Z. Zhu, F. Qin, J. Bao, M. J. Yacaman, P. M. Ajayan, D. Chen and J. M. Tour, *Nat. Commun.*, 2015, **6**, 8668.
- 44 Z. Chen, Z. Duan, Z. Wang, X. Liu, L. Gu, F. Zhang, M. Dupuis and C. Li, *ChemCatChem*, 2017, **9**, 3641–3645.